Journal of Volcanology and Geothermal Research 259 (2013) 133–144

Contents lists available at SciVerse ScienceDirect

Journal of Volcanology and Geothermal Research

journal homepage: www.elsevier.com/locate/jvolgeores

Doppler weather radar observations of the 2009 eruption of Redoubt Volcano, Alaska

David J. Schneider [a,*], Richard P. Hoblitt [b]

[a] U.S. Geological Survey, Alaska Volcano Observatory, 4230 University Dr, Anchorage, AK 99508, United States
[b] U.S. Geological Survey, Cascades Volcano Observatory, 1300 SE Cardinal Ct. Vancouver, WA 98683, United States

ARTICLE INFO

Article history:
Received 13 July 2011
Accepted 2 November 2012
Available online 16 November 2012

Keywords:
Radar
Redoubt Volcano
Tephra
Explosive eruptions
Aggregation

ABSTRACT

The U.S. Geological Survey (USGS) deployed a transportable Doppler C-band radar during the precursory stage of the 2009 eruption of Redoubt Volcano, Alaska that provided valuable information during subsequent explosive events. We describe the capabilities of this new monitoring tool and present data captured during the Redoubt eruption. The MiniMax 250-C (MM-250C) radar detected seventeen of the nineteen largest explosive events between March 23 and April 4, 2009. Sixteen of these events reached the stratosphere (above 10 km) within 2–5 min of explosion onset. High column and proximal cloud reflectivity values (50 to 60 dBZ) were observed from many of these events, and were likely due to the formation of mm-sized accretionary tephra-ice pellets. Reflectivity data suggest that these pellets formed within the first few minutes of explosion onset. Rapid sedimentation of the mm-sized pellets was observed as a decrease in maximum detection cloud height. The volcanic cloud from the April 4 explosive event showed lower reflectivity values, due to finer particle sizes (related to dome collapse and related pyroclastic flows) and lack of significant pellet formation. Eruption durations determined by the radar were within a factor of two compared to seismic and pressure-sensor derived estimates, and were not well correlated. Ash dispersion observed by the radar was primarily in the upper troposphere below 10 km, but satellite observations indicate the presence of volcanogenic clouds in the stratosphere. This study suggests that radar is a valuable complement to traditional seismic and satellite monitoring of explosive eruptions.

Published by Elsevier B.V.

1. Introduction

The rapid detection of explosive volcanic eruptions and accurate determination of eruption-column altitude and ash-cloud movement are critical factors in the mitigation of volcanic risks to aviation and in the forecasting of ash fall on nearby communities. Volcanic ash transport and fallout models are used to forecast the hazards posed by volcanic ash, but their use requires estimates of eruption source parameters (Mastin et al., 2009). The parameters that can typically be estimated in real-time include explosion onset time, cloud altitude and duration. Other factors such as vertical mass distribution and particle size distribution are not easily constrained during eruption response. Weather radar has been used to provide basic eruption observations (Harris and Rose, 1983; Rose et al., 1995; Oswalt et al., 1996; Lacasse et al., 2004; Tupper et al., 2005) and more recently to provide quantitative estimates of eruptive mass (Marzano et al., 2006a, 2006b, 2010).

All of these previous studies have utilized permanent radar systems, which typically are not optimized for volcano monitoring due to their primary mission of providing meteorological observations. This paper reports on the initial deployment of a transportable radar system dedicated to monitoring explosive activity at Redoubt Volcano in 2009. Radar complements traditional seismic monitoring of volcanoes by providing real-time all weather observation capabilities. When correlated with seismic data, it provides unambiguous evidence that ash is being erupted. The use of radar at a volcano observatory is ideal as these data are more easily merged with traditional geophysical data sources. Furthermore, radar data compliments satellite-based observations of eruptive activity by providing timely observations (minutes versus tens of minutes to hours for satellite observations), accurate cloud height measurement (unlike satellite-based thermal infrared techniques that can provide ambiguous estimates), and sensitivity to different particle sizes (hundreds of microns to mm-sized, versus tens of microns and smaller for thermal infrared satellite).

1.1. Overview of Redoubt Volcano and the 2009 eruption

Redoubt Volcano is an ice-clad stratovolcano located about 170 km southwest of Anchorage, Alaska and within 100 km of communities on the Kenai Peninsula (see Bull and Buurman, 2013 for additional details concerning the location, setting, and overview of Redoubt Volcano and the 2009 eruption). Anchorage serves as the transportation hub for Alaska and has a major and critical role in air cargo traffic between North America and Asia. The summit of Redoubt Volcano is 3108 m above sea level (asl), but historical eruptive activity in 1966–68, 1989–90, and 2009 has taken place from vents in an ice-filled crater at about 2400 m asl. The previous eruption in

* Corresponding author. Tel.: +1 907 786 7037; fax: +1 907 786 7425.
E-mail address: djschneider@usgs.gov (D.J. Schneider).

0377-0273/$ – see front matter. Published by Elsevier B.V.
http://dx.doi.org/10.1016/j.jvolgeores.2012.11.004

1989–90 resulted in a significant aircraft encounter with a volcanic ash cloud that nearly resulted in a crash (Guffanti et al., 2010). This incident highlighted the need for rapid eruption detection, forecasting of cloud movement, and communication of hazards to aviation. Many improvements in the capabilities of the responsible agencies in Alaska were made during the intervening 20 years to improve the safety of flight, while not unnecessarily restricting operations.

Unrest at Redoubt Volcano began during the summer of 2008, and by early 2009 increases and/or changes in a variety of volcano monitoring parameters indicated a high probability of an explosive eruption (Schaefer, 2012). The increase in the severity of unrest at Redoubt, its explosive history, and potential to adversely affect air traffic in Alaska and across the North Pacific lead to the deployment by the U.S. Geological Survey of a dedicated volcanic ash monitoring radar system. The first small phreatic explosion occurred at Redoubt on March 15, 2009, followed by nineteen larger magmatic explosions between March 23 and April 4, 2009. The nineteen largest explosions were assigned a sequential number by Alaska Volcano Observatory (AVO) as described in Bull and Buurman (2013), and these identifying numbers are used in this manuscript. Additional smaller explosions are described by McNutt et al. (2009), and were too small to be detected by the methods described below.

2. Methods and data

This study reports on the first deployment of a transportable Enterprise Electronics Corporation MiniMax-250C (MM-250C) Doppler radar in Kenai, Alaska for the dedicated purpose of monitoring eruptive activity at Redoubt Volcano (Fig. 1). Comparisons are made with Weather Surveillance Radar-1988, Doppler (WSR-88D) data products from radar site PAHG, located about 10 km north of the MM-250C site, seismic and pressure sensor data, thermal infrared satellite data, and tephra-fall deposits.

2.1. The MM-250C radar system

The MM-250C Doppler radar operates in the C-band (5.36 cm) and has a 2.4-meter parabolic antenna with a beam width of 1.6°, a transmitter power of 250 W, and a maximum effective range of 240 km. The entire disassembled system, including a radome, fits inside a 20-foot steel shipping container that has been modified to serve as base for the antenna/radome, and as a field station for observers and other monitoring equipment (Fig. 1). Other specifications of the system are shown in Table 1.

Fig. 1. MM-250C Doppler radar system deployed at the Kenai Municipal Airport.

Table 1
Specifications of the EEC MM-250C meteorological radar used in this study.

Parameter	Specification
Wavelength (C-band)	5.35 cm
Polarization	Horizontal
Transmit power	250 W
Pulse length	1.6 μs
Pulse repetition frequency	1000 Hz
Range	100 km
Gate width	250 m
Antenna	2.4 m parabolic
Beam width	1.6° (2.6 km at 82 km range)
Scan speed (45° sector)	~15 s per elevation angle

The radar was installed at the Kenai Municipal Airport, 82 km east of Redoubt and operated remotely from the Alaska Volcano Observatory office in Anchorage (Fig. 2). In addition to a 180-degree unobstructed view of the volcano, this secure site offered the support of the airport staff and the City of Kenai. A further advantage was the proximity of Federal Aviation Administration WSR-88D NEXRAD Doppler radar located about 10 km N of the Kenai Airport and operated by the National Weather Service Anchorage Forecast Office. This permitted comparisons with an established weather-monitoring radar system.

The MM-250C became fully operational about 1 day prior to the first explosive eruption on March 23, 2009. The radar was primarily operated in a sector volume mode, utilizing a 45-degree sector centered on Redoubt (Fig. 2). During some events, the azimuth of the sector being scanned was modified to track the drifting ash cloud. The sector scanning strategy allowed for high temporal resolution. Each elevation angle required 15 s to complete, versus 2 min for a complete 360-degree scan. The number of elevation angles in a sector scan volume varied from 7 to 10 during the 2009 eruption resulting in full sector volumes being collected every 105 to 150 s, respectively.

A typical vertical scanning strategy utilizing 8 elevation angles with beam centers from 2.0 to 12.5° is shown in Fig. 3. Central radar

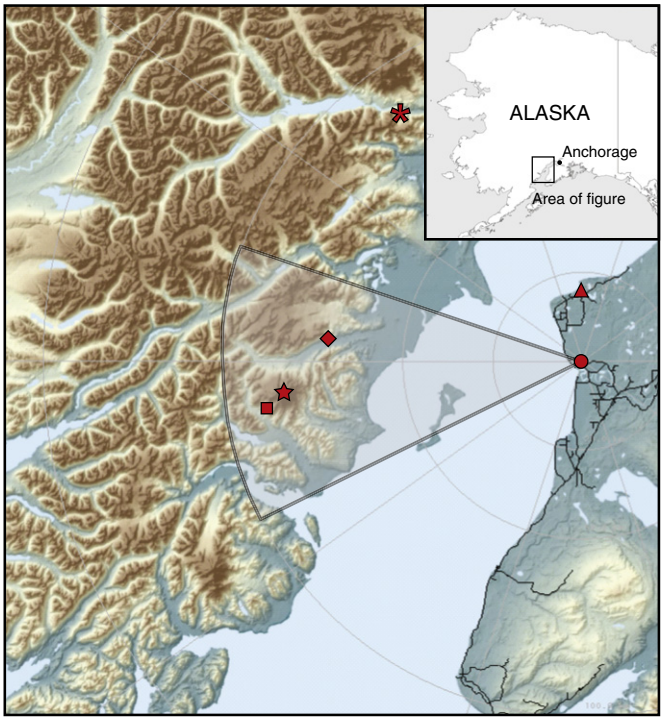

Fig. 2. Map showing the location of the MM-250C radar (circle), NEXRAD site PAHG (triangle), Redoubt Volcano (star), seismic station RB03 (square), pressure sensor DFR (diamond), and seismic station SPU (asterisk). The typical scanning coverage, 45° sector and 100 km range, are indicated by the shaded area.

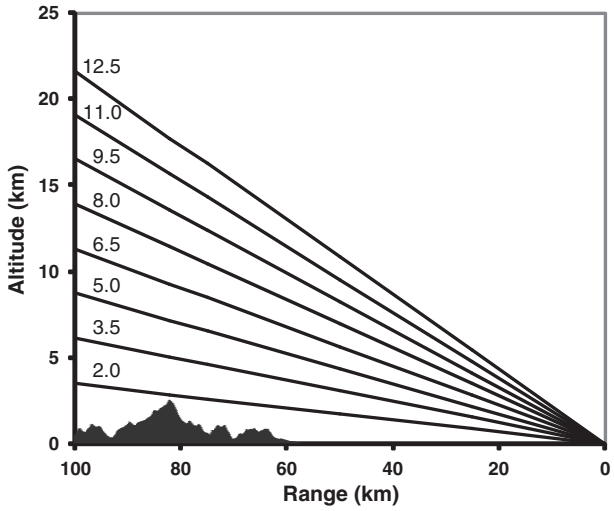

Fig. 3. Typical vertical scanning strategy used to produce sector volumes showing the relationship between scan angles and central beam height. Topographic profile shows the location of Redoubt Volcano at range of 82 km.

beam height H was calculated utilizing a standard atmospheric refraction model as outlined by Rinehart (2004), using the following equation:

$$H = \sqrt{r^2 + R^2 + 2rR\sin\varnothing} - R + H_o \quad (1)$$

where r is the range from the radar to the point of interest, R is 4/3 the radius of the earth, $\varnothing$ is the elevation angle, and H_o is the height of the radar above sea level (30 m). The down-range distance from the radar to Redoubt was 82 km, producing central beam heights from 2.9 to 17.7 km above sea level for the scan elevation angles shown in Fig. 3. The summit elevation of Redoubt is 3108 m, but the eruptive vent is at approximately 2400 m and topography prevented direct observation of the vent by the radar beam. Note that the radar-derived eruption cloud height values given in this paper are for the central beam height (above sea level) and the true values may be as much as 2 km higher. This is due to uncertainty in how much of the radar beam (2 km high at the volcano) is filled by volcanic ash. If the beam is completely filled, the cloud height would be about 1 km greater, however as much as 1/2 of the next higher beam could contain volcanic ash without it being observed as a radar return.

2.2. Estimate of ash detection capability

Like many meteorological radars, the MM-250C transmits a pulse of energy, and then passively listens for the return of energy scattered by particles. In a simplified form without signal loss, the intensity of received power P_r can be calculated using the Probert–Jones equation (Probert-Jones, 1962):

$$P_r = \frac{R_c|K|^2 z}{r^2} \quad (2)$$

where R_c is the radar constant (includes the transmit power, antenna gain, angular beamwidth, pulse length, and transmitted energy wavelength), K is the particle dielectric factor, z is the radar reflectivity factor, and r is the range from the radar to the point of interest. For Rayleigh scattering conditions (particle diameter less than 5.35 mm for the MM-250C) the radar reflectivity factor z is defined as:

$$z = \sum N_i D_i^6 \quad (3)$$

where N_i is the number of particles of diameter D_i per unit volume. Thus, the received power is highly dependent upon particle size. Radar reflectivity factor (z) spans many orders of magnitude, so it is typically converted to logarithmic reflectivity factor (z) and expressed in units of dBZ by:

$$Z = 10\log\ (z). \quad (4)$$

The relationship between ash particle size, ash mass concentration and logarithmic reflectivity factor (Z) was calculated and the results are shown in Fig. 4. In these calculations, the simplified target volume is assumed to be composed entirely of spherical ash particles with a particle density of 2.0 g/cm^3, and a dielectric factor of 0.39 (Adams et al., 1996) for volcanic ash. Note that the results are for a simplified target volume that does not account for a variable particle size distribution within the volume. The MM-250C has minimum detectable reflectivity of approximately 20 dBZ at the range of 82 km (the distance from the radar site to Redoubt), and this field is indicated by the shaded portion of the plot shown in Fig. 4. For volcanic cloud mass concentrations greater than 1 g/m^3, only particles with a diameter greater than 0.6 mm would be detectable. Very fine-grained ash (diameter of 0.01 mm) which can stay airborne for many days is likely not detectable by the MM-250C.

3. Results and discussion

3.1. Eruption column height

There were nineteen explosive events between March 23 and April 4, 2009 that are summarized in Table 2. Of these, sixteen had radar-derived maximum eruption column heights in excess of 9 km above sea level, the approximate altitude of the boundary between the troposphere and the stratosphere at the time of the events. The MM-250C was able to detect the eruption column of the seventeen largest and highest events, and the maximum column heights were similar to those detected by the WSR-88D radar (Fig. 5). The WSR-88D was able to detect two smaller explosive events, including the onset of explosive activity on March 23, 2009, due to its much higher power and greater sensitivity to low reflectivity eruption clouds. Eruption-cloud heights generally increased through Event 8 at 17:26 UTC on March 26, after which time the maximum cloud height was lower and relatively

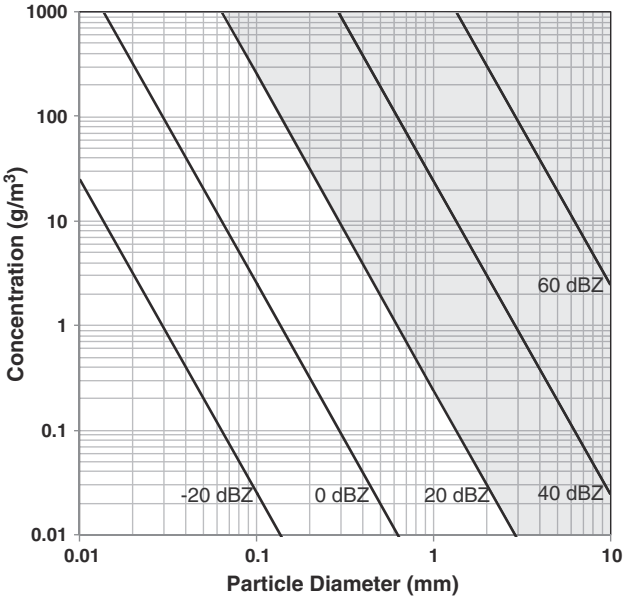

Fig. 4. Relationship between particle diameter (mm), ash mass concentration (g/m^3), and logrithmic radar reflectivity factor (dBZ). The shaded portion of the plot indicates the variation in particle diameter and mass concentration values that can be detected by the MM-250C at a range of 82 km.

Table 2
Explosive events, maximum eruption column heights derived from MM-250C and WSR-88D radars, and event durations as estimated by MM-250C radar, local pressure sensor DFR, and distant seismic sensor SPU.

Explosive event	Start time[a] (UTC)	MM-250C height (km)	WSR-88D height[b] (km)	MM-250C duration[c] (min)	Pressure duration[d] (min)	Seismic duration[e] (min)
1	3/23/09 06:35	Not detected	5.5	Not detected	26	2
2	3/23/09 07:02	14.3	13.4	6	3	7
3	3/23/09 08:14	15	13.1	9	13	20
4	3/23/09 09:39	13.6	13.1	17	8	38
5	3/23/09 12:31	16.4	14.9	13	16	20
6	3/24/09 03:41	17.8	18.3	16	12	15
7	3/26/09 16:34	8.6	6.7	Not determined	1	Not detected
8	3/26/09 17:24	19.2	18.9	13	7	14
9	3/27/09 07:47	12.9	11.0	3	15	Not detected
10	3/27/09 08:29	15	14.9	11	4	7
11	3/27/09 16:39	15	15.5	5	4	8
12	3/28/09 01:35	15	11.9	2	2	2
13	3/28/09 03:25	15	15.2	3	3	4
14	3/28/09 07:20	12.9	11.9	3	2	2
15	3/28/09 09:20	15	13.1	4	2	2
16	3/28/09 21:40	Not detected	5.2	Not detected	2	6
17	3/28/09 23:29	12.9	12.2	3	3	6
18	3/29/09 03:23	15	12.5	4	4	11
19	4/04/09 13:55	15	14.9	16	31	31

[a] Eruption start times from S. McNutt (personal communication, May 11, 2011).
[b] Heights from WSR-88D Level III echo tops data product.
[c] Estimated using methodology described in Section 3.4.
[d] S. McNutt (personal communication, May 11, 2011).
[e] Power et al. (2013).

constant at 13–15 km above sea level. Fee et al. (2013) report a significant shift in acoustic activity for events 10–18, but the relationship between their acoustic observations and our radar observed eruption-cloud height observations will require further study.

Radar data were the primary source of eruption cloud height information used in public warning messages from the Alaska Volcano Observatory (AVO) and the National Weather Service (NWS) during the 2009 eruption of Redoubt Volcano (Schaefer, 2012). Heights from the WSR-88D were used as the official eruption cloud heights, as the accuracy of that system was well established. The MM-250C system provided significant additional operational awareness to the staff of the AVO involved in the eruption response. This included more rapid and more frequent observations of the eruption-column (compared to the WSR-88D), which greatly decreased uncertainty in interpreting seismic signals associated with explosive activity. In many cases, verbal eruption notifications were made to the Federal Aviation Administration (FAA) Alaska Regional Traffic Control Center and the NWS Alaska Aviation Weather Unit while the eruption column was still ascending. Ash dispersion forecasts were made and airborne ash hazard warnings were issued by the NWS using radar data to characterize the maximum eruption cloud heights.

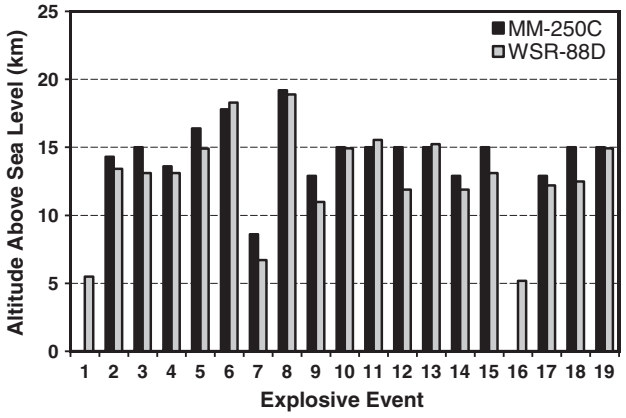

Fig. 5. Comparison between maximum cloud height determined by the MM-250C and WSR-88D for nineteen explosive events of Redoubt Volcano between March 23 and April 4, 2009.

3.2. Radar reflectivity observations

We use reflectivity data from event numbers 5 and 19 to illustrate the typical images collected by the MM-250C. Event 5 is representative of the discrete, short-duration explosive events that characterized the first five closely-spaced magmatic explosions that occurred within 6 h on March 23. The initial events removed a small dome that had grown in the summit amphitheater, and the subsequent explosions excavated a large area of rock and glacial ice. In contrast, the last explosion (event 19) on April 4 was associated with the collapse and removal of a moderate sized dome (Bull and Buurman, 2013). The distribution of tephra-fall deposits from these two events were the best constrained of all of the explosive events as they did not overlie or mix with other fall deposits (Wallace et al., 2013). Eruption onset times were determined by S. McNutt (personal communication, May 11, 2011) through analysis of local pressure sensor data. Seismic records are from broadband station RD03 located 5 km southwest of the vent. All heights are given in km above sea level.

3.2.1. Explosive event 5

The onset time for event 5 was 12:30:21 UTC on 23 March, 2009. Fig. 6A shows a time-series of reflectivity cross sections through the eruption cloud from (approximately) south to north; Fig. 6B shows the seismic record from RD03 (Fig. 2), and Fig. 7 shows the associated Plan Position Indicator (PPI) images at an altitude of 7.9 km above sea level. Within two minutes of onset, the eruption cloud reached a height of 6.5 km (Fig. 6A) and was initially characterized by relatively low reflectivity values (<30 dBZ). Over the next three scan intervals (about 4.5 min), the altitude of the eruption cloud rose rapidly to 16.4 km by 12:37 UTC, and the reflectivity values in the core of the column increased to a value of about 55 dBZ. The cloud height began to decrease by 12:38 although the core of high reflectivity values persisted through 12:43 UTC. Over the next 7.5 min, the reflectivity at the eruptive vent continued to decline, and the maximum reflectivity values were observed to the north of the vent in the

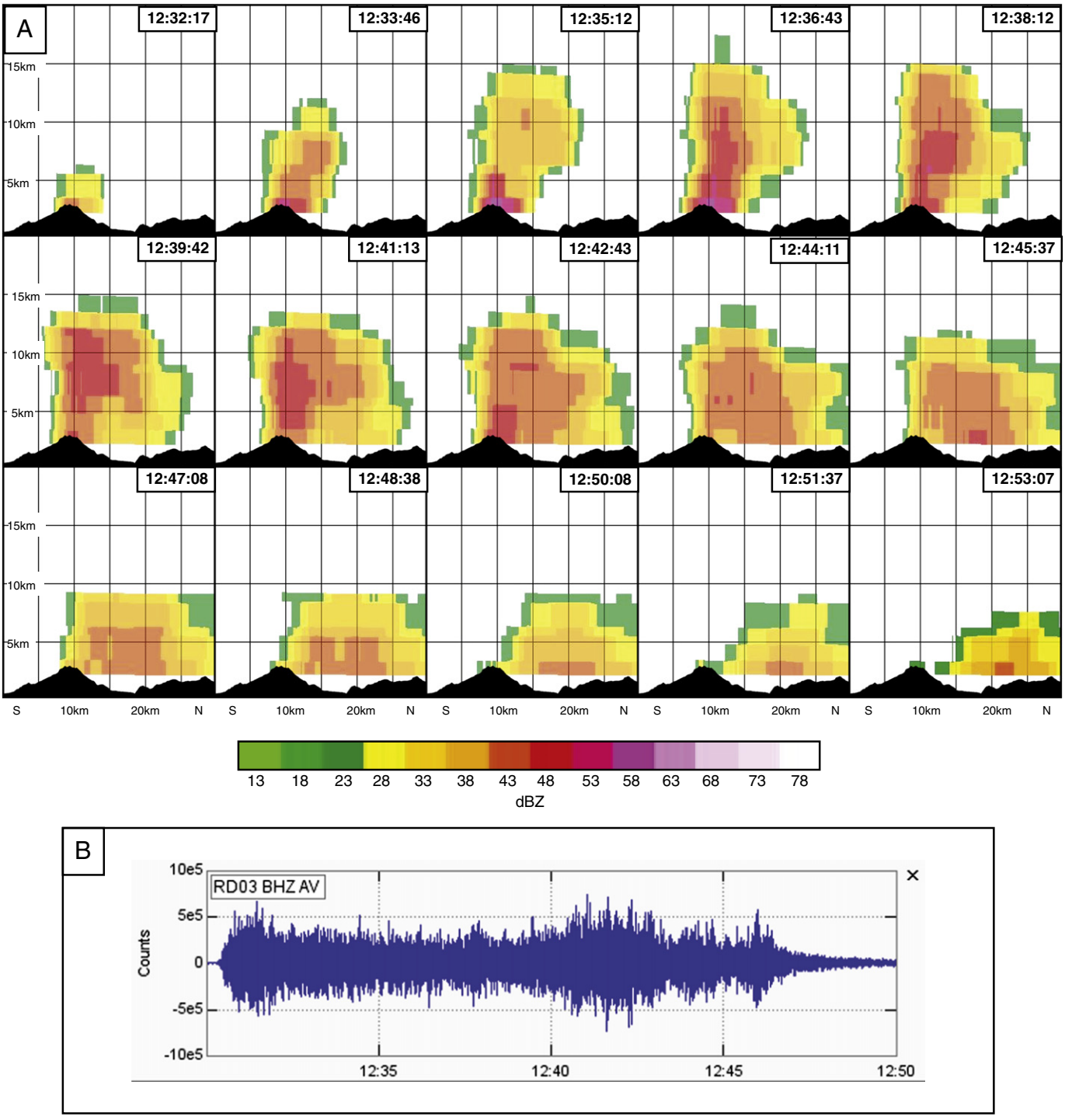

Fig. 6. A) Reflectivity cross sections through eruption cloud from event 5 on March 23, 2009. Times in UTC for start of volume scan, which take 90 s to complete. Location of cross-section is shown in Fig. 7. B) Seismic record of explosive event 5 from temporary broadband seismometer RD03, located 5 km southwest of the vent.

dispersing ash cloud. The cloud height decreased rapidly during this time period, at a rate of about 10 m/s.

The seismic record from station RB03 shows an impulsive start to this explosive event (Fig. 6B), followed by relatively uniform amplitude through about 12:40:30, when the amplitude increases. This increase in amplitude does not correspond to any noticeable increase in detected cloud height, and occurs as the reflectivity values near the vent begin to decline.

The PPI images at an altitude of 7.9 km (Fig. 7) show a roughly circular eruption cloud characterized by a high reflectivity core that decreases towards the cloud edge. Movement of the cloud at this altitude is primarily towards the north with lesser expansion to the east and west. The reflectivity values at this altitude decrease rapidly after 12:43 UTC and are barely detectable by 12:53 UTC. The rapid decrease in reflectivity at this altitude is likely due to the fallout of lapilli tephra and a decrease in the cloud ash concentration.

All of the detected explosive events, with the exception of event 19, shared broadly similar reflectivity patterns and evolution. This includes rapid cloud rise, high central core reflectivity values (50–60 dBZ), and rapid decrease in cloud reflectivity and height once the eruptive event ended. The drifting clouds were typically only observable in the MM-250C data for tens of minutes following the eruption end, with

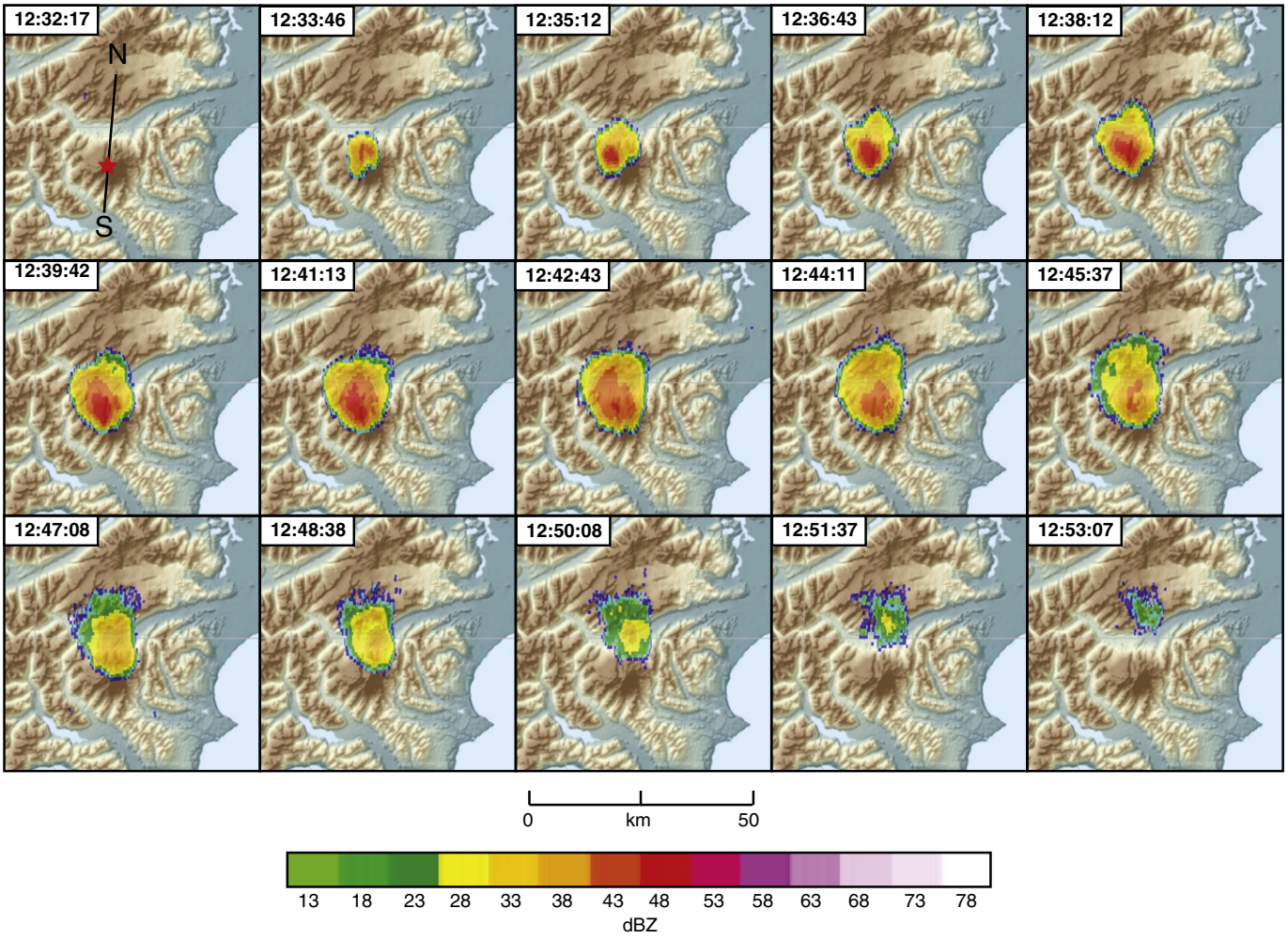

Fig. 7. Plan Position Indicator reflectivity images at an altitude of 7.9 km above sea level of the eruption cloud from event 5 on March 23, 2009. Times in UTC for start of volume scan, which take 90 s to complete. Position of the vent is shown by the red star, and the location of the north–south cross-section shown in Fig. 6 is indicated by the line.

the exception of the cloud from event 17 on 28 March which moved to the east (towards the radar).

3.2.2. Explosive event 19

The last major explosive event of the 2009 eruption, number 19, began on April 4, 2009 at 13:57:05 UTC (S. McNutt, personal communication, May 11, 2011) and destroyed a moderate-sized lava dome that had grown since March 29. Fig. 8A shows a time-series of reflectivity cross sections through the eruption cloud during the first 30 min of the event from northwest to southeast, Fig. 8B shows the seismic record from RD03, and Fig. 9 shows the associated Plan Position Indicator (PPI) images at an altitude of 6.4 km above sea level. This event was more complex than most of the other explosions, and was characterized by pulses of activity as seen in the cloud height, reflectivity, and seismic amplitude.

At the onset of event 19, the eruption cloud was characterized by relatively low reflectivity values (<30 dBZ) which rose more slowly than the cloud from event 5 (and most other explosive events) as seen in Fig. 8A. Within 10 min of the eruption onset, the cloud had reached an altitude of about 15 km, and exhibited a modest increase in the reflectivity at the vent (<40 dBZ). The cloud height varied over the next 20 min, but was generally from 10 to 15 km. The seismicity shows a similarly emergent signal at the onset of the eruption, and two phases of increased amplitude. The radar observations are generally in good agreement with the seismicity recorded during this event (Fig. 8B). An increase in the radar reflectivity after 14:15 corresponds to an increase in seismic amplitude, and the overall decline in seismic amplitude after 14:25 corresponds to a decrease in reflectivity. The maximum cloud height decreased rapidly at a rate of ~25 m/s from 14:11 to 14:15:30 and ~17 m/s from 14:25 to 14:30. This is about 2–2.5 times faster than that observed in the cloud from event 5. The fallout deposits from event 19 were finer-grained than those from event 5 (Wallace et al., 2013), suggesting that the observed decrease in cloud height may be due to an overall decrease in cloud concentration rather than rapid sedimentation of lapilli tephra.

The volcanic ash from this event was transported to the southeast (Fig. 9) and resulted in significant ash fall on communities on the east side of Cook Inlet. Unfortunately, the sector scanning strategy that focused on activity at the volcano resulted in the ash cloud moving out of the field of view of the radar (indicated by the dashed line in Fig. 9). Although the region of high reflectivity values near the vent (>50 dBZ) was much smaller for event 19 than for event 5 (Fig. 7) the reflectivity signal downwind was higher and was observed for a longer period of time.

3.3. Eruption cloud rise rate

The eruption cloud rise rate for sixteen explosive events was determined from the maximum cloud altitude as a function of time after eruption onset. The timing of the altitude observations is based on the specific scan angles within which the cloud tops were observed; eruption onset times are from S. McNutt (personal communication, May 11, 2011). The results are given in Fig. 10, and show that the vertical velocity of the eruption cloud tops ranged from 25 to 60 m/s. The rise rate from

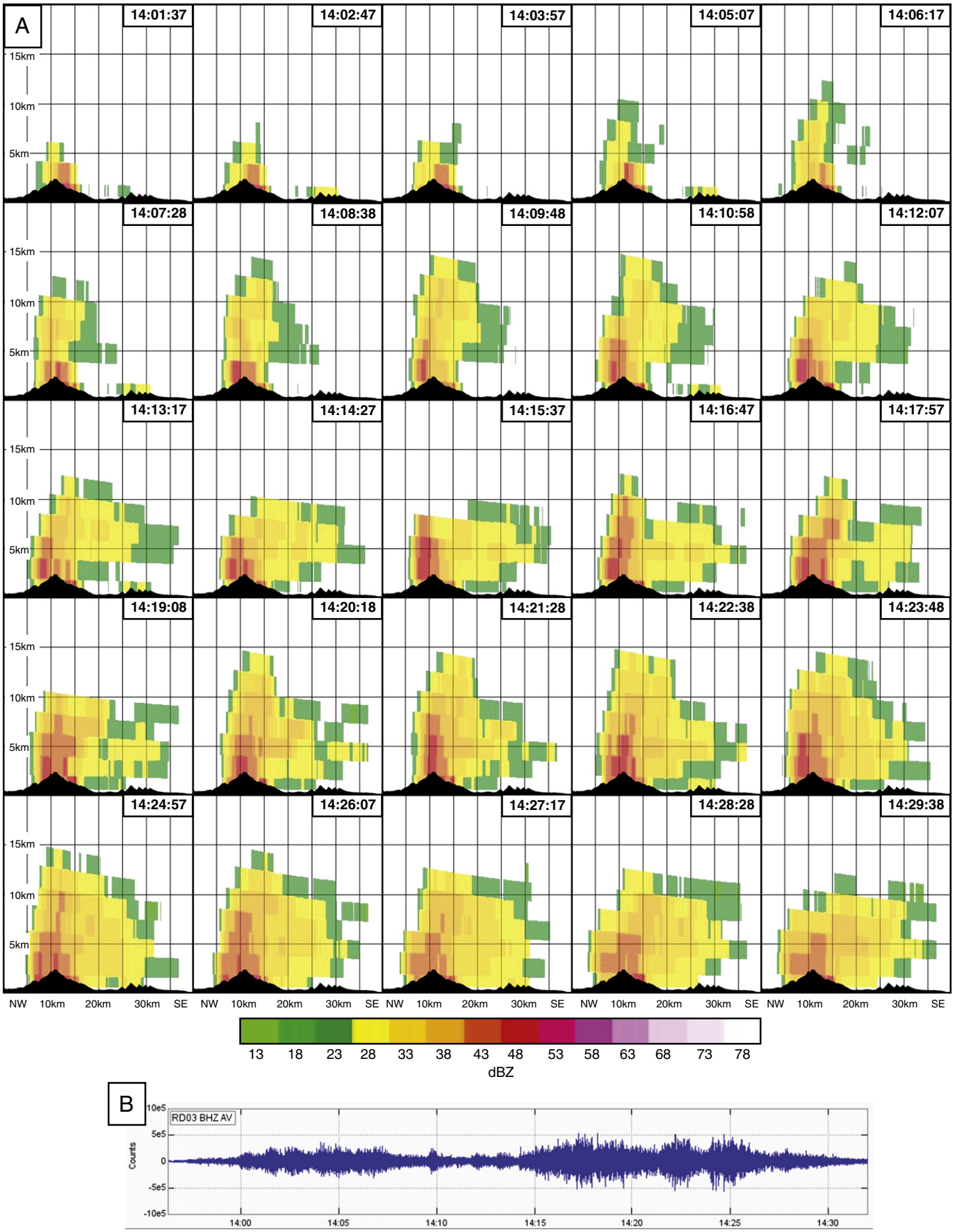

Fig. 8. A) Reflectivity cross sections through eruption cloud from event 19 on April 4, 2009. Times in UTC for start of volume scan, which take 70 s to complete. Location of cross section is shown in Fig. 9. B) Seismic record of explosive event 5 from temporary broadband seismometer RD03, located 5 km southwest of the vent.

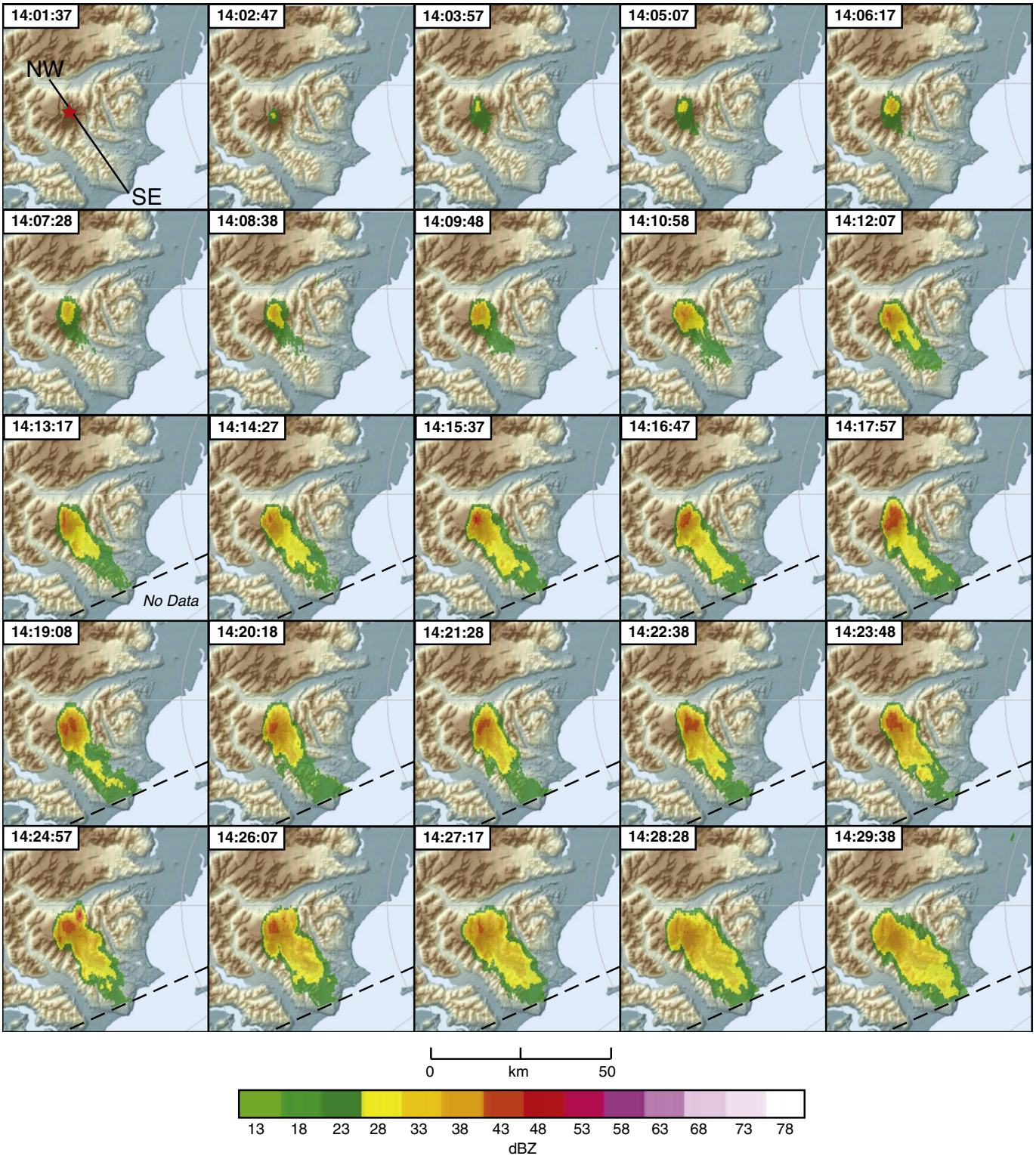

Fig. 9. Plan position indicator reflectivity images at an altitude of 6.4 km above sea level of the eruption cloud from event 19 on April 4, 2009. Times in UTC for start of volume scan, which take 70 s to complete. Position of the vent is shown by the red star, and the location of the northwest–southeast cross-section shown in Fig. 8 is indicated by the line. The edge of the scan sector is indicated by the dashed line.

event 5 and the first fifteen minutes of event 19 are highlighted. Note that most of the clouds reached jet aircraft cruise altitudes (~10 km above sea level) within 2 to 5 min of eruption onset, with the exception of the eruption cloud from event 19 which rose slowly for the first 7 min before increasing rapidly. The eruption cloud rise rates from these events are typical for explosive events and reinforce the need for rapid cloud height determination to help mitigate the hazard to aviation.

3.4. Eruption duration estimates

Eruption duration is a source parameter required by volcanic ash dispersion models, but can be difficult to estimate in near-real time. Methods for estimating duration from seismic and pressure sensors typically use the increase in amplitude for a seismic or pressure wave above some background value. These estimates can be made

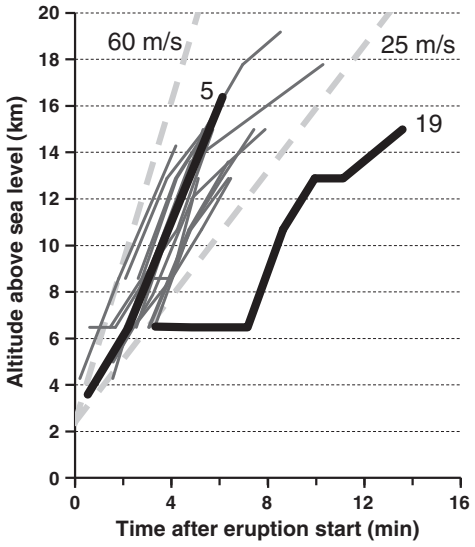

Fig. 10. MM-250C radar-derived cloud heights versus time after eruption start for sixteen explosive events at Redoubt Volcano between March 23 and April 4, 2009. Data from explosive events 5 and 19 are labeled and indicated by the thicker lines. Velocities of 25 m/s and 60 m/s are shown by the dashed lines for reference.

from local or distant stations and typically provide a range of values. Radar can provide a direct observation of reflecting particles in the eruption column and may be used to help constrain duration. However, radar reflectivity images show a combination of ash emissions in the column as well as ash fallout which complicates the interpretation. Eruption durations were estimated from the MM-250C data by observing the timing of reflectivity values in excess of 40 dBZ at a height of 6 km above the vent. The reflectivity threshold was chosen to identify periods of high concentrations of large particles, and the height and location was chosen to reduce the influence of ash fallout. Note that radar-derived eruption durations are dependent upon the inherent sensitivity of the radar system, and thus the chosen threshold is not universal. These estimates were compared to seismic (Power et al., 2013) and pressure-derived (S. McNutt personal communication, May 11, 2011) durations and the results are shown in Table 2 and Fig. 11.

In general, the duration estimates from the seismic and atmospheric pressure approaches are within a factor of 2 of the radar-derived estimates. Fig. 11A shows the comparison between the radar-derived duration with the duration derived from seismic station SPU, located 85 km north of Redoubt. At this distance, the effects of surface processes such as pyroclastic flows and lahars on the seismic amplitude are negligible. A linear regression of these data yield an $R^2 = 0.64$. Fig. 11B shows the relationship between pressure sensor-derived duration estimates from station DFR (located 15 km NE of Redoubt) and the radar-derived estimates. The agreement between these techniques is worse with an $R^2 = 0.36$. The better fit with the seismic data suggests a slightly better coupling between the seismic energy recorded at a distant station and ash emission than for pressure waves at a proximal station, but this is not definitive. The variability in the various estimates of eruption duration illustrates the uncertainty and difficulty in estimating eruption source parameters for ash dispersion, transport and fallout models.

3.5. Comparisons to satellite data

One of the surprising aspects of the 2009 eruption of Redoubt was the height of the eruption clouds as determined by the MM-250C and NEXRAD radars. These estimates are generally consistent with each other, and document that as many as sixteen events produced volcanic clouds that entered into the stratosphere. Satellite data provide additional evidence for the cloud height as estimated by radar observations. As volcanic clouds rise in the atmosphere, they equilibrate to the ambient temperature. The standard technique for estimating cloud height is to compare the cloud top temperature to a temperature profile of the atmosphere. This works well for clouds emplaced in the troposphere, but it is more problematic for those volcanic clouds that have enough upward momentum to enter the stratosphere. In those cases, the temperature inversion that exists at the troposphere-stratosphere boundary results in multiple solutions for the temperature comparison method.

Fig. 12A shows an AVHRR thermal infrared satellite image of the volcanic cloud from explosive event 5, imaged at 13:36 UTC on 23 March, 2009 (about one hour after eruption onset). At the time of this image, the volcanic cloud has become elongated along a NW-SE line in a sector to the north and east of the volcano. The central region of the cloud is still opaque in the thermal infrared, as suggested by the fringe of warmer temperature values along the cloud edge; thus the temperature values derived from this portion of the cloud are

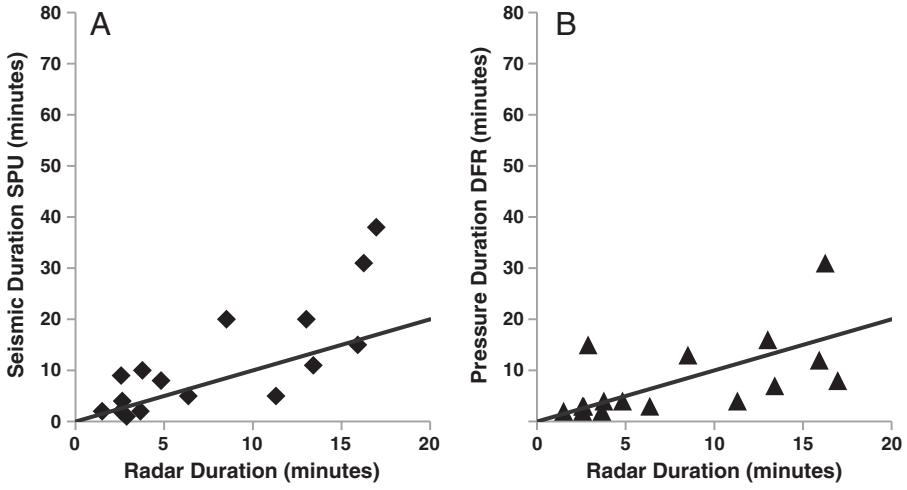

Fig. 11. Eruption duration estimates for sixteen explosive events at Redoubt Volcano between March 23 and April 4, 2009. A) MM-250C radar-derived duration versus seismic duration from distant station SPU located 85 km north of Redoubt. B) MM-250C radar-derived duration versus pressure sensor duration from local station DFR located 15 km northeast of Redoubt. The solid line is for a 1:1 ratio between duration estimates.

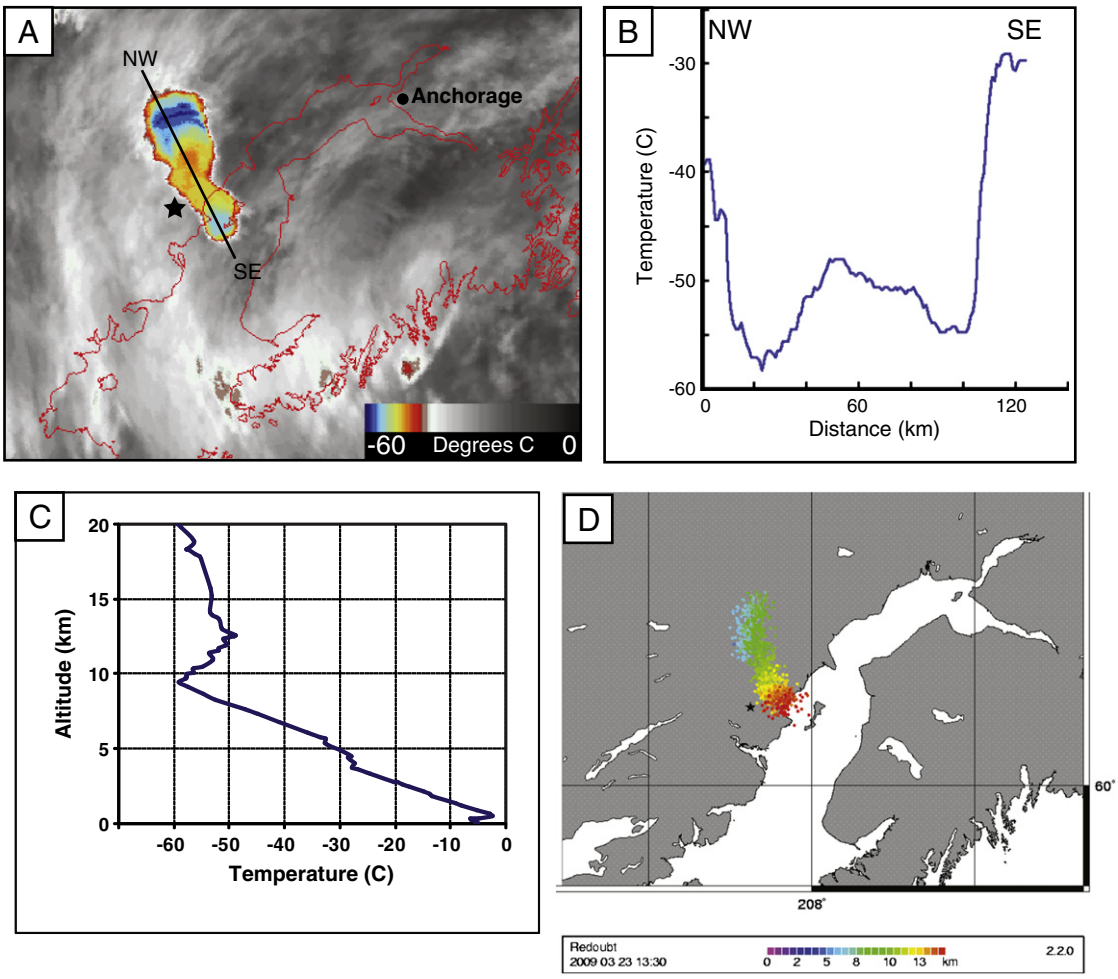

Fig. 12. A) AVHRR thermal infrared satellite image of volcanic cloud from event 5, imaged at 13:36 UTC on 23 March 2009. Location of Redoubt shown by the star and orientation of northwest–southeast temperature profile shown by the line. B) Temperature profile along northwest–southeast line from AVHRR image. C) Temperature–altitude plot from radiosonde launched in Anchorage at 12:00 UTC on 23 March, 2009. D) PUFF dispersion model output showing altitude of cloud tracer particles that range in height from 6 to 16 km above sea level. Image is from forecast time of 13:30 UTC to match AVHRR image.

representative of the cloud top and are not affected by warmer clouds beneath it. The coldest portion of the volcanic cloud is about −58 °C and is located to the northwest (Fig. 12B), is warmer (−48 to −52 °C) in the central portion, and then colder (−55 °C) in the southeastern portion. By comparing these temperature values to a profile (Fig. 12C) collected by radiosonde launched in Anchorage at 12:00 UTC, the altitude of the cloud can be estimated. These data suggest the northwest portion of the cloud was near the tropopause at an altitude of about 9.5 km above sea level, the central warmer portion was about 12–14 km, and the southerly colder portion was about 16–17 km. These observations strongly suggest that this volcanic cloud entered the stratosphere, and additional evidence is provided by comparison to cloud movement and PUFF ash transport model output (Searcy et al., 1998). The PUFF results are shown in Fig. 12D, and agree quite well with the temperature and radar-derived cloud height observations shown in Fig. 6A. Although the mapped ash fallout from event 5 was primarily to the north (Wallace et al., 2013; Mastin et al., 2013), this and subsequent satellite images (Webley et al., 2013; Steensen et al., 2013) show that a volcanogenic cloud was observed dispersing at the altitude observed by the radar.

3.6. Comparison to tephra-fall deposits

The tephra-fall deposits from the explosive events were mapped, sampled, and analyzed by Wallace et al. (2013). In many cases it was not possible to differentiate the deposits from individual events due to the overlapping nature of the deposits from closely spaced explosions and lack of snow-fall between events. Fall deposits from events 5 and 19 were among the best differentiated permitting comparisons with radar data.

Terminal settling velocities were calculated for a range of particle diameters to help constrain comparative interpretations of the radar data and the tephra-fall deposits, and the results are shown in Fig. 13. These calculations are for spherical particles with a density of 2.0 g/cm^3, and utilize atmospheric properties from radiosonde data collected at Anchorage, Alaska on March 23, 2009 at 1200 UTC. Note that particles larger than several mm in diameter have terminal velocities in excess of 10 m/s at an altitude of 15 km.

3.6.1. Explosive event 5

Fall-deposits from explosive event 5 were found primarily to the north of the volcano, and were mapped to a distance in excess 300 km, at a mass density of 10 g/m^2. In contrast, the MM-250 radar data was only able to observe the dispersed cloud for a distance of about 30 km from the source, which was well within the 1000 g/m^2 maximum contour of Wallace et al. (2013). The most proximal sample was located about 12 km from the vent, had a mass of about 6,500 g/m^2, and was comprised almost entirely of accretionary tephra-ice pellets up to 8 mm in diameter. The large size of these accretionary pellets account for the high radar reflectivity observed (>55 dBZ). A rapid decrease in cloud height was observed following the end of the eruption (>10 m/s), and is good agreement with the terminal settling velocities

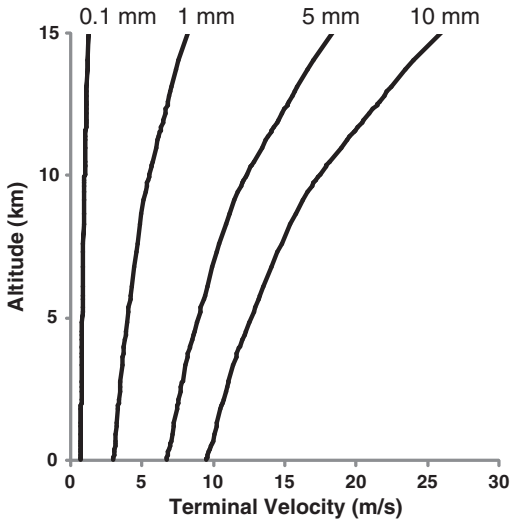

Fig. 13. Terminal settling velocities for spherical particles of various diameters as a function of altitude. A particle density of 2.0 g/cm^3 was utilized and atmospheric properties were determined from radiosonde data collected at Anchorage, Alaska on March 23, 2009 at 1200 UTC.

shown in Fig. 13. The radar observation strongly suggest that the process of accretionary pellet formation occurred very rapidly (<10 min) in the column and proximal portion of the eruption cloud. Abundant lightning was detected during this, and all other explosive events (Behnke et al., 2013), and accretionary pellet formation may have played a key role in the electrical charge separation process.

Particle size analyses of the proximal deposits show that the accretionary pellets found within the field of view imaged by the MM-250C radar contained a significant mass fraction of fine-grained ash particles (Wallace et al., 2013). The distal cloud was depleted in fine-grained ash because of the proximal scrubbing. The relative lack of fine-grained ash may account for the relatively poor thermal infrared brightness temperature signals (Wen and Rose, 1994) observed for many of the volcanic clouds from the 2009 eruption (Steensen et al., 2013; Webley et al., 2013), and possibly from the 1989–90 eruption (Schneider and Rose, 1994).

C-band radar observations of the 1992 eruption of the Crater Peak vent of Mount Spurr conducted using a more powerful radar at a similar distance showed lower maximum column reflectivity values of about 30 dBZ (Rose et al., 1995) than those observed using the MM-250C radar during the 2009 eruption of Redoubt. The resulting volcanic clouds from the Spurr eruption were easily tracked with satellite brightness temperature difference images (Schneider et al., 1995), suggesting that fine-grained ash was not removed by particle accretion in the column. These observations suggest that it may be possible to identify accretion in the column and proximal cloud by the high radar reflectivity, rapid decrease in observed radar height, and analysis of satellite thermal infrared brightness temperature difference data.

3.6.2. Explosive event 19

Tephra-fall deposits from explosive event 19 were found more than 150 km to the southeast of Redoubt and resulted in minor ash fall (<2 mm thickness) in communities on the east side of Cook Inlet (Wallace et al., 2013). These deposits were finer-grained than those from previous events of similar volume, and are interpreted to have been generated by dome collapse and related pyroclastic flows (Wallace et al., 2013). This interpretation is reinforced by the radar reflectivity cross-sections (Fig. 8A). Many images acquired after 14:13:17 exhibit maximum reflectivity values to the north of the vent, where pyroclastic flows ran out into the Drift River valley. The fine-grained nature of the ash from this event is suggested by the lower reflectivity values observed near the vent (compared to event 5), and the longer downwind extent of the dispersed ash cloud. The rapid rate of decrease (~17 to 25 m/s) and fluctuation of the observed eruption cloud height (Fig. 8) may be due to the inability of the MM-250C radar to detect the fine-grained ash except when the mass concentration was very high. Very large particles (>10 mm as shown in Fig. 13) would be required to replicate the observed fall rates, either as individual particles or accretionary pellets, but these are not observed in the deposits. Such large particles would have high radar reflectivity values (≫ 50 dBZ), but the downwind reflectivity values were relatively low (25–35 dBZ). Further evidence of the absence of enhanced removal of fines due to accretionary pellet formation can be observed in the satellite thermal infrared brightness temperature images, which show a significantly more robust signal compared to the volcanic cloud from event 5 (Steensen et al., 2013). The cloud observed by the MM-250C lies within the mapped 4000 g/m^2 contour as interpreted by Wallace et al. (2013). Unfortunately, the sector scanning strategy employed during this event resulted in the area of the detected cloud being truncated, so the maximum extent of the observable cloud is not known.

4. Conclusions

The use of MM-250C and WRS-88D meteorological radars during the 2009 eruption of Redoubt Volcano provided invaluable information to aid in the operational response and observed a variety of volcanological phenomena. The temporal resolution of the MM-250C data is unprecedented in weather radar remote sensing of explosive eruptions. Rapid eruption cloud rise was observed and further documented the ascent of potentially hazardous volcanic ash to aviation flight levels within minutes of onset. This highlights the unique utility of radar systems to provide this information in real-time. Sixteen explosive eruptions reached altitudes in excess of 10 km above sea level and injected ash and volcanic gases into the stratosphere. These heights were considerably greater than would traditionally be estimated using thermal infrared satellite data which use the coldest observed cloud temperature. Volcanic clouds that enter the stratosphere can be significantly warmer than those in the troposphere, and this study suggests that cloud height would have been underestimated if not for the use of radar. Analysis of cloud dispersion confirms the presence of volcanogenic clouds in the stratosphere. The availability of abundant water may explain the observed heights, but additional column dynamics modeling is needed to confirm this speculation. High radar reflectivity values in the column and proximal cloud, as well as the rapid decrease in cloud altitude and high reflectivity values strongly suggest that the formation of accretionary tephra-ice pellets (observed in many of the fall deposits) occur very rapidly in the first minutes of eruption onset. Accretionary pellet formation scrubs fine-grained ash from the resultant dispersed cloud and may result in poor thermal infrared satellite based detection of the ash clouds from the 2009 and possibly from the 1989–90 eruption as well.

Acknowledgments

The authors wish to thank the City of Kenai, Alaska and especially Mary Bondurant and Earl Hicks from the Kenai Municipal Airport for their generous and unqualified support in the installation of the MM-250C. We could not have found a better site for the radar nor better people with which to work. We would also like to thank Matthew Logan, Greg Speer, John Paskievitch, Cyrus Read, and Stuart Wilkinson from the USGS Volcano Science Center for their aid in designing and installing the radar system. Installing a brand new system in Alaska in the winter has its challenges and this team worked to overcome them all. Finally, we would like to thank the reviewers of this manuscript for their helpful comments.

References

Adams, R.J., Perger, W.F., Rose, W.I., Kostinski, A., 1996. Measurements of the complex dielectric constant of volcanic ash from 4 to 19 GHz. Journal of Geophysical Research 101, 8175–8185.

Behnke, S.A., Thomas, R.J., McNutt, S.R., Schneider, D.J., Krehbiel, P.R., Rison, W., Edens, H.E., 2013. Observations of volcanic lightning during the 2009 eruption of Redoubt Volcano. Journal of Volcanology and Geothermal Research 259, 214–234.

Bull, K.F., Buurman, H., 2013. An overview of the 2009 eruption of Redoubt Volcano, Alaska. Journal of Volcanology and Geothermal Research 259, 2–15.

Fee, D., McNutt, S., Arnoult, K., Szuberla, C., Olson, J., Lopez, T., 2013. Combining local and remote infrasound recordings from the 2009 Redoubt Volcano eruption. Journal of Volcanology and Geothermal Research 259, 100–114.

Guffanti, M., Casadevall, T.J., Budding, K., 2010. Encounters of aircraft with volcanic ash clouds. A Compilation of Known Incidents, 1953–2009: U.S. Geological Survey Data Series 545. ver. 1.0, http://pubs.usgs.gov/ds/545.

Harris, D.M., Rose, W.I., 1983. Estimating particle sizes, concentrations, and total mass of ash in volcanic clouds using weather radar. Journal of Geophysical Research 88, 10969–10983.

Lacasse, C., Karlsdóttir, S., Larsen, G., Soosalu, H., Rose, W.I., Ernst, G.G.J., 2004. Weather radar observations of the Hekla 2000 eruption cloud, Iceland. Bulletin of Volcanology 66, 457–473.

Marzano, F.S., Barbieri, S., Vulpiani, G., Rose, W.I., 2006a. Volcanic ash cloud retrieval by ground-based microwave weather radar. IEEE Transactions on Geoscience and Remote Sensing 44, 3235–3246.

Marzano, F.S., Vulpiani, G., Rose, W.I., 2006b. Microphysical characterization of microwave radar reflectivity due to volcanic ash clouds. IEEE Transactions on Geoscience and Remote Sensing 44, 313–327.

Marzano, F.S., Marchiotto, S., Barbieri, S., Textor, C., Schneider, D., 2010. Model-based weather radar remote sensing of explosive volcanic ash eruption. IEEE Transactions on Geoscience and Remote Sensing 48, 3591–3607.

Mastin, L.G., Guffanti, M., Servranckx, R., Webley, P., Barsotti, S., Dean, K., Denlinger, R., Durant, A., Ewert, J.W., Neri, A., Rose, W.I., Schneider, D., Siebert, L., Stunder, B., Swanson, G., Tupper, A., Volentik, A., Waythomas, C.F., 2009. A multidisciplinary effort to assign realistic source parameters to models of volcanic ash-cloud transport and dispersion during eruptions. Journal of Volcanology and Geothermal Research 186, 10–21.

Mastin, L.G., Schwaiger, H., Schneider, D.J., Wallace, K.L., Schaefer, J.R., Denlinger, R.P., 2013. Injection, transport, and deposition of tephra during event 5 at Redoubt Volcano, 23 March, 2009. Journal of Volcanology and Geothermal Research 259, 201–213.

McNutt, S.R., Arnoult, K., Olson, J.V., Szuberla, C., West, M.E., Clark, E., 2009. Local infrasound observations of the explosive eruptions of Redoubt Volcano, Alaska, March–April 2009. AGU Fall Meeting Abstracts, A2213.

Oswalt, J.S., Nichols, W., O'Hara, J.F., 1996. Meteorological observations of the 1991 Mount Pinatubo eruption. In: Newhall, C.G., Punongbayan, R.S. (Eds.), Fire and Mud: Eruptions and lahars of Mount Pinatubo, Philippines. Philippine Institute of Volcanology and Seismology, University of Washington Press, Quezon City, Seattle, pp. 625–636.

Power, J.A., Stihler, S.D., Chouet, B.A., Haney, M.M., Ketner, D.M., 2013. Seismic observations of Redoubt Volcano, Alaska — 1989–2010 and a conceptual model of the. Redoubt magmatic system 259, 31–44.

Probert-Jones, J.R., 1962. The radar equation in meteorology. Quarterly Journal of the Royal Meteorological Society 88, 485–495.

Rinehart, R.E., 2004. Radar for Meteorologists, 4th edition. Rinehart Publications, Columbia, MO, p. 66.

Rose, W.I., Kostinski, A.B., Kelley, L., 1995. Real time C band radar observations of 1992 eruption clouds from Crater Peak/Spurr volcano, Alaska. In: Keith, T.E.C. (Ed.), The 1992 Eruptions of Crater Peak Vent, Mount Spurr Volcano, Alaska: U. S. Geological Survey Bulletin, 2139, pp. 19–26.

Searcy, C., Dean, K., Stringer, W., 1998. PUFF: a high-resolution volcanic ash tracking model. Journal of Volcanology and Geothermal Research 80, 1–16 http://dx.doi.org/10.1016/S0377-0273(97)00037-1.

Schaefer, J.R. (Ed.), 2012. The 2009 Eruption of Redoubt Volcano, Alaska, Alaska Division of Geological & Geophysical Surveys Report of Investigations 2011–5.

Schneider, D.J., Rose, W.I., 1994. Observations of the 1989–90 Redoubt Volcano Eruption Clouds using AVHRR Satellite Imagery. In: Casadevall, T.J. (Ed.), Volcanic ash and aviation safety; proceedings of the First international symposium on Volcanic ash and aviation safety: U. S. Geological Survey Bulletin, 2047, pp. 405–418.

Schneider, D.J., Rose, W.I., Kelley, L., 1995. Tracking of 1992 eruption clouds from Crater Peak vent of Mount Spurr Volcano, Alaska, using AVHRR. In: Keith, T.E.C. (Ed.), The 1992 eruptions of Crater Peak vent, Mount Spurr Volcano, Alaska: U. S. Geological Survey Bulletin, 2139, pp. 27–36.

Steensen, T., Stuefer, M., Webley, P.W., Grell, G., Freitas, S., 2013. Qualitative comparison of Mount Redoubt 2009 volcanic clouds using the PUFF and WRF-Chem dispersion models and satellite remote sensing data. Journal of Volcanology and Geothermal Research 259, 235–247.

Tupper, A., Oswalt, J.S., Rosenfield, D., 2005. Satellite and radar analysis of volcanic-cumulonimbi at Mount Pinatubo, Philippines, 1991. Journal of Geophysical Research 110, D9204 http://dx.doi.org/10.1029/2004JD005499.

Wallace, K., Schaefer, J., Coombs, M., 2013. Character, mass, distribution, and origin of tephra-fall deposits from the 2009 eruption of Redoubt Volcano, Alaska—Highlighting the significance of particle aggregation. Journal of Volcanology and Geothermal Research 259, 145–169.

Webley, P.W., Lopez, T.M., Dean, K.G., Rinkleff, P., Dehn, J., Cahill, C.F., Wessels, R., Ekstrand, A., Bailey, J.E., Izbekov, P., Worden, A., 2013. Remote observations of eruptive clouds and surface thermal activity during the 2009 eruption of Redoubt volcano. Journal of Volcanology and Geothermal Research 259, 185–200.

Wen, S., Rose, W.I., 1994. Retrieval of sizes and total masses of particles in volcanic clouds using AVHRR bands 4 and 5. Journal of Geophysical Research 99, 5421–5431.